Presented at e^+e^- Factories 1999, Sept. 21-24, 1999, KEK Laboratory **CBN 99-30**

Beam-Generated Detector Backgrounds at CESR *

Stuart Henderson †, Laboratory of Nuclear Studies, Cornell University, Ithaca NY, 14853, USA
David Cinabro, Wayne State University, Detroit MI, 48202, USA

Abstract

The CESR/CLEO Phase II interaction region is described. The operational experience with beam-generated detector backgrounds is reviewed. The status of our understanding of beam-generated detector backgrounds at CESR is described and comparisons of background measurements with simulation predictions are presented.

1 INTRODUCTION

A new CESR/CLEO interaction region [1, 2] was installed in 1995 as part of the CESR Phase II upgrade. At the same time the CLEO experiment [3] installed a silicon vertex detector (SVX) around a 2 cm radius beryllium beampipe, and new detector shielding. (The new configuration of the CLEO detector is referred to as CLEO II.V[4]) The use of radiation sensitive SVX readout electronics located just outside the central beampipe placed a premium on accurate prediction and understanding of beam-related detector backgrounds at CESR. This article describes the detector shielding system, commissioning and operational experience and presents a status report on our present understanding of beam-generated detector backgrounds at CESR.

The CESR Phase II interation region (IR) was optimized for bunch train collisions at a small horizontal crossing angle (see [5] in these proceedings). CESR presently operates with 9 trains of bunches, each of which consists of 4 bunches spaced by 14 ns. The peak stored beam current to date is 550 mA with nearly equal electron and positron beam currents.

The dominant CLEO detector background arises from lost particles generated by bremsstrahlung interactions with the residual gas within about 30 m of the IP. Coulomb scattering is a small contribution as is the dose from scattered synchrotron radiation. The CLEO experiment is sensitive to beam-generated backgrounds through the following mechanisms: i) background hits (detector occupancy) in the drift chambers, ii) background hits (occupancy) in the SVX, iii) radiation dose to the SVX readout electronics, iv) radiation dose to the CsI crystal calorimeter and v) increased data-acquisition trigger rates. It turns out that the radiation sensitivity of the silicon readout electronics (CAMEX amplifiers) placed the most stringent requirements on the maximum tolerable detector background rates. Radiation damage studies [6] found that the failure dose for the powered CAMEX amplifiers is $\sim$25 krad ($\sim$100 krad unpowered). For detector shielding design purposes we chose the following design criteria: i) SVX layer 1 occupancy $< 1\%$ hits/strip/μs, and ii) SVX readout electronics dose < 20 krad in 3 years.

2 CESR PHASE II INTERACTION REGION

2.1 Design Considerations

The crossing angle orbit has important consequences for synchrotron radiation backgrounds. The incoming beam is off-axis in the interaction region quadrupoles, perhaps by as much as 1 cm, generating substantial SR power only a few meters from the IP. This source alone would lead to unacceptably large detector backgrounds. In order to bring the incoming beam nearer the axis of the nearest horizontally focusing quadrupole, the beam is displaced horizontally with a magnetic IP displacement bump. This bump was included in the lattice design phase to ensure adequate aperture. With the use of this bump, SR powers are reduced and with proper shielding the background rates are acceptable. In addition, for injection the beams are separated horizontally at the IP, again placing one beam off-axis in the IR quads and producing higher SR fluxes during injection than HEP.

The detector background shielding system was designed based on the results of detector background simulations which were developed for lost particles and synchrotron radiation. These simulations are described in detail elsewhere[2, 7]. The results of these simulations were compared to detector background measurements performed with CLEO-II and were found to be in very good agreement providing confidence in their predictive power [8, 9, 10, 7].

2.2 Detector Shielding

The detector shielding consists of two parts. The detector is shielded from lost beam particles by a large tungsten mask approximately 2.5 cm thick extending from $\sim$24 cm to $\sim$50 cm from the IP. In addition, the rare-earth permanent magnet quadrupole material provides additional shielding outboard of the tungsten mask. Tungsten was selected as the mask material because of its short radiation length. The detailed shape was designed based on the results of Monte-Carlo simulations of beam-gas scattering.

* Work supported by the National Science Foundation.
† Email: sdh9@cornell.edu

The detector is shielded from synchrotron radiation by a stepped copper mask. The innermost mask tip is located at $r = 1.2$ cm and $z = 26$ cm. The mask is profiled in such a way that SR photons strike only the tips of the mask structure; the surfaces parallel to the beam direction are angled slightly so that these surfaces intercept no SR flux that would otherwise forward scatter into the detector beampipe. As a result, all incoming SR power is absorbed on the tips. Rather than make these tip surfaces at right angles to the beam direction, the surfaces are sloped to reduce the HOM power generated in the structure. The slope is small enough that the tip surfaces remain hidden from the detector beampipe. Thus, the background from SR arises from photons which scatter through a mask tip ("tipscattering") and photons which pass over the innermost mask tip and strike the downstream surface of the mask and subsequently scatter into the beampipe ("backscattering").

The central detector beampipe [11] is a double-walled water cooled beryllium beampipe with inner radius $r = 1.9$ cm. To further reduce the SR backgrounds a 10 μm gold coating was deposited [12] on the inner surface of the beampipe. The coating reduces the radiation dose to the SVX detector by 3-4 orders of magnitude. To further reduce the lost particle background the innermost mask tip is made of tantalum rather than copper. Since during injection one of the beams is off-axis in the IR quads, the possibility for large SR fluxes exists. A set of retractable tungsten foil radiation shields are mounted to the beampipe. These tungsten shields were closed during CESR injection for the first year of operation, and then were left open during HEP operations and closed during machine studies.

In order to reduce beam-gas scattering near the IR new vacuum chambers and pumping was installed within ± 12 m of the IP. IR Pumping is accomplished in large plenums which incorporate massive titanium sublimation pumping [13]. Pumping plenums are located at $\pm$ 2m, $\pm$ 6 m, and $\pm$ 10 m from the IP.

Detector backgrounds are monitored with two systems. The first is a PIN diode radiation monitoring system mounted directly on the ends of the beryllium beampipe. Twelve diodes are mounted on each end and are uniformly distributed in azimuth. This system is sensitive to both charged particles and SR photons. Another system, consisting of a set of CsI crystals placed in the CLEO endcaps, is useful for monitoring charged particle backgrounds.

The background simulation predictions for design currents (600 mA total) and a 40% duty factor are given in Table 1. Both the expected dose and occupancy are below the design goals mentioned above. As can be seen the beam-gas background dominates.

Table 1: Detector background simulation results for 600 mA total current and a 40% duty factor.

Source	SVX layer 1 Occ. % hits/layer/μs	Dose krad/year
SR	0.002	0.64
Beam-Gas	0.18	8
Total	0.18	9

3 OPERATIONAL EXPERIENCE

3.1 Total Dose and Average Rates

CLEO II.V ran for a total of 172 weeks from 29 October 1995 until 15 February 1999. The first month was completely devoted to machine studies, the next two months to a detector engineering run, but after that the detector ran continously for three years. There were eight scheduled maintenance periods lasting, on average, three and a half weeks and three unscheduled periods each of less than one week. The integrated running time of the detector was 142 weeks. During that time the total accumulated radiation dose measured by the beampipe PIN diode monitors was 22.2 krads. Of that, 14.8 krads were logged when CESR was delivering luminosity to CLEO and 12.0 krads when CLEO was actually taking data. The dose when CESR was not delivering luminosity was dominated by injection, and amounts to 3.6 krads. This implies that injection for luminosity represents 30% of the dose logged in data taking. The balance of the dose was logged in machine studies (3.5 krads) and during the short time spent between injection and HEP data-taking (0.3 krads). Most of the dose during machine studies ($\sim$75%) was logged during injection. The integrated dose versus month of running is shown in Figure 1.

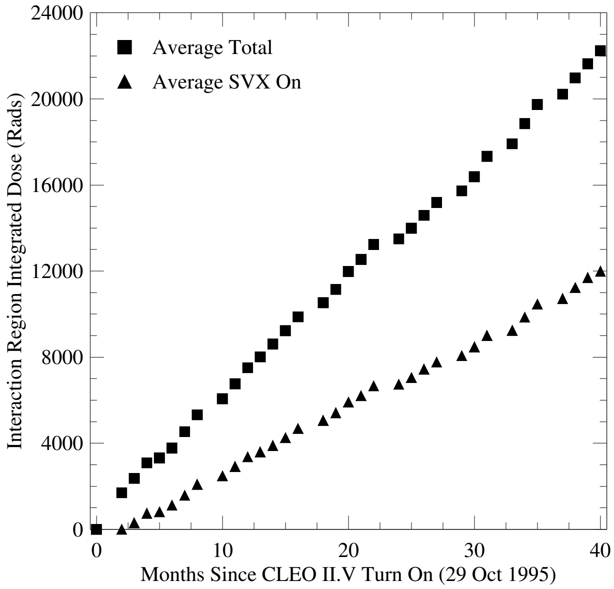

Figure 1: The integrated interaction point dose versus month of CLEO II.V running.

During the course of the CLEO II.V run CESR delivered 11.6 fb^{-1} of luminosity and CLEO logged 9.0 fb^{-1}. The total Amp-Hours accumulated during the CLEO II.V run was just over 4000. These imply that the total dose rates were 0.16 krads/running week, 1.9 krads/fb^{-1} delivered, 2.5 krads/fb^{-1} logged, and 5.6 rads/Amp-Hour. Based on these numbers and the expected radiation hardness of the SVX readout electronics the detector could have survived for 30% longer. We did have one readout chip fail in the way expected from radiation damage; a sudden increase in noise in all the channels in the chip was observed in the last six months of running. This chip was in layer 3 where lower quality chips were used, but the dose rate was expected to be more than a factor of two smaller than that observed by the PIN diode system which is located near layer 1.

During the Phase II IR commissioning period, 2.4 krads were accumulated in the first three months with only 155 A-hr. There are several reasons for this high specific dose rate. The dynamic pressure rise (dP/dI) was naturally large during this period since new vacuum chambers were installed in the IR. In addition, much of the time was spent tuning high current injection which has a higher dose rate than colliding beam running. This startup period represented a dose/A-hr about three times what was achieved in normal running.

4 COMPARISON OF MEASUREMENTS WITH SIMULATION

4.1 Pressure Bump Studies

Controlled pressure bump studies are among the most important tests of the beam-gas background simulation since such tests check directly the model of the source-effectiveness for scattered beam particles. By source-effectiveness we mean the relative contibution to detector background due to beam-gas scattering at a particular location in the ring. The source-effectiveness for SVX layer 1 hits predicted by the beam-gas simulation is shown in Figure 2. (Reference [14] in these proceedings shows another source effectiveness calculation, that for IR mask strikes.) The actual background is therefore the source-effectiveness weighted by the pressure profile scaled appropriately by the beam current.

We have performed such studies by turning off pumps near the IR to generate pressure bumps and by introducing calibrated leaks. We report on one such study in which a calibrated N_2 leak was introduced 12 m from the IP. A series of "pump conditions" was generated by turning off successive pumps near the IR [16]. Pressures were recorded for each pump condition. These data were used together with a model of pumping in the IR (described in [14] in these proceedings) to generate a predicted pressure profile. Pressure profiles for seven pump conditions predicted by the model are shown in Figures 3 and 4. The detector radiation dose was measured for each of these seven conditions. The pressure profiles together with the source-effectiveness and known beam current provide a simulation prediction of the radition dose for each of the pump conditions. The comparison is shown in Figure 5. We take the good agreement as confirmation that the beam-gas source-effectiveness predicted by the simulation is correct.

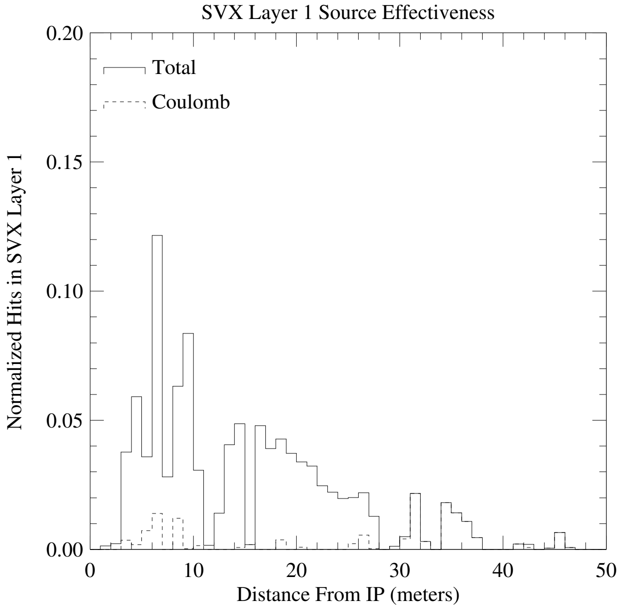

Figure 2: The source effectiveness distribution. This plot shows the relative contribution to the SVX layer 1 occupancy from beam-gas scattering as a function of scatter (source) position.

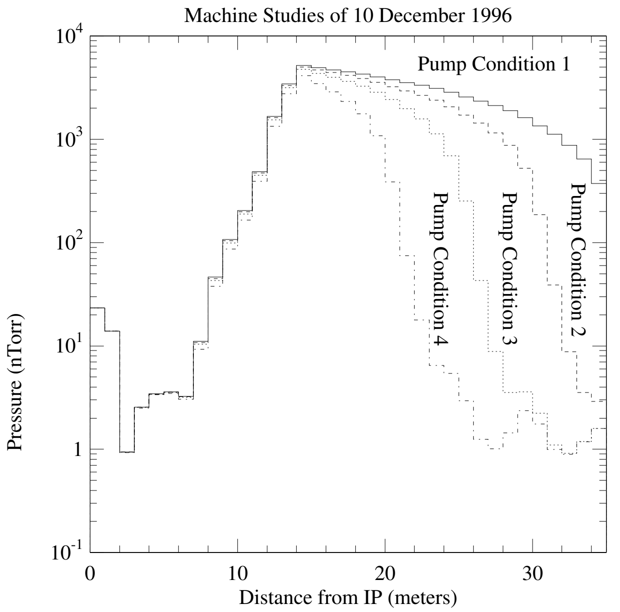

Figure 3: Pressure distribution near the CESR/CLEO II.V interaction region during a controlled leak pressure bump study for various vacuum pump conditions.

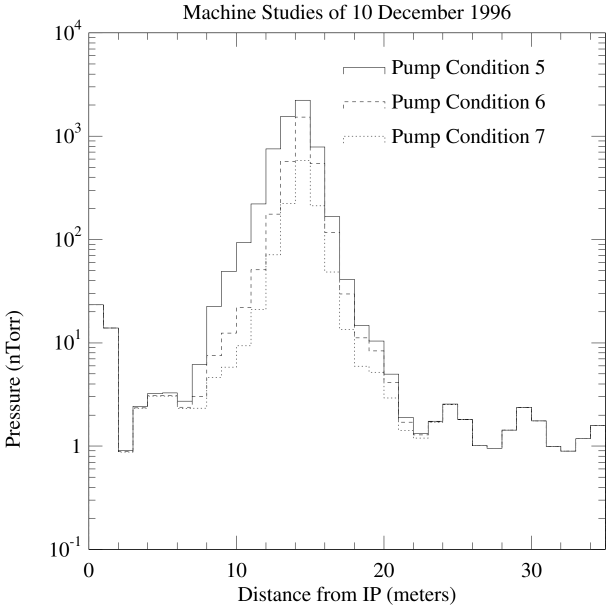

Figure 4: Pressure distribution near the CESR/CLEO II.V interaction region during a controlled leak pressure bump study for various vacuum pump conditions.

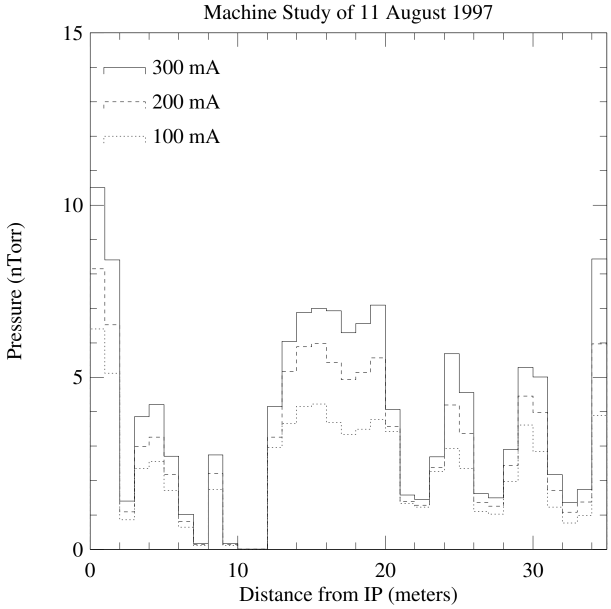

Figure 6: The calculated pressure profile near the CESR/CLEO II.V IR during HEP running.

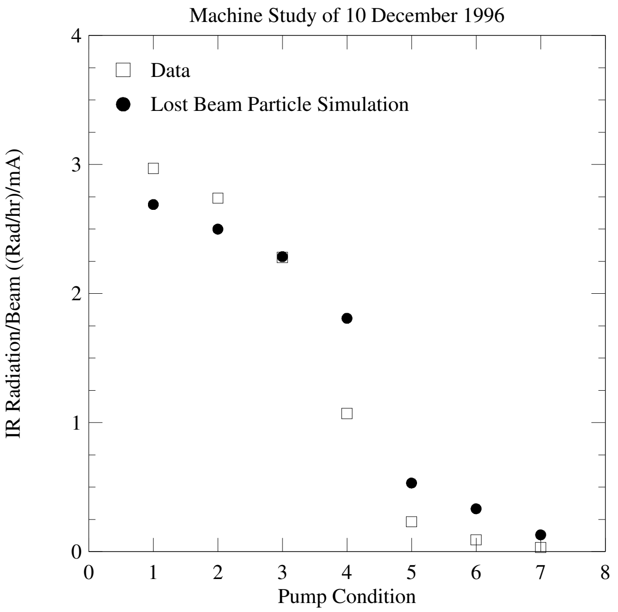

Figure 5: Radiation dose rate at the CESR/CLEO II.V IP for the seven pump conditions shown in Figures 3 and 4 compared with the prediction of the beam-gas simulation.

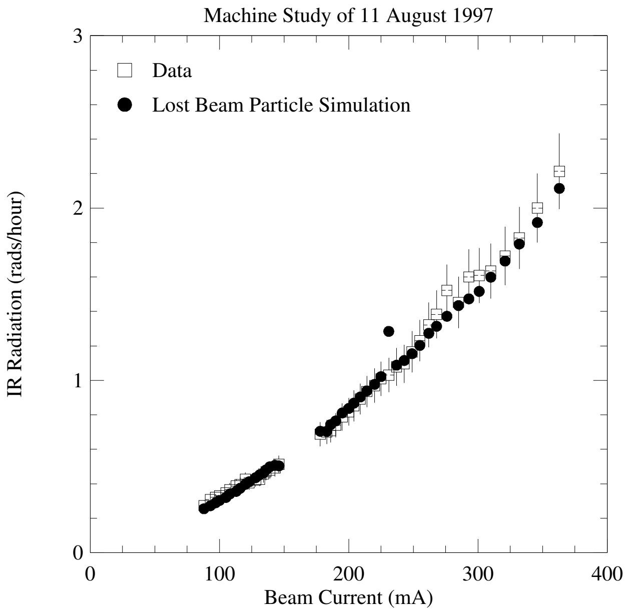

Figure 7: The radiation level at the CESR/CLEO II.V IP during HEP running. The prediction of the lost beam particle simulation and the measured data are shown.

4.2 *High Energy Physics Running*

We can also check the prediction of our simulation in standard high energy physics (HEP) running conditions. This prediction depends on the pressure distribution which is taken from a calculation[15] done at a beam current of 300 mA. The extrapolation to different beam currents is done by assigning the pressure measurements (cold-cathode gauges or ion pump currents) to regions of the beamline and appropriately scaling with beam current. The pressure distributions used by the simulation for HEP running are shown in Figure 6 for various beam currents. The pressure distribution is combined with the source effectiveness and beam current to give the background levels as a function of beam current. Figure 7 shows the radiation level at the IP. The agreement is striking.

Since HEP data was also taken during this test we can compare the measured and predicted occupancy levels in the CLEO II.V detector. The measured and predicted SVX layer 1 occupancy are shown in Figure 8. The occupancy is measured in terms of hits/strip/event where the integration time of an "event" is about 8 μs in the SVX. The agreement here is good, but is complicated by many confounding

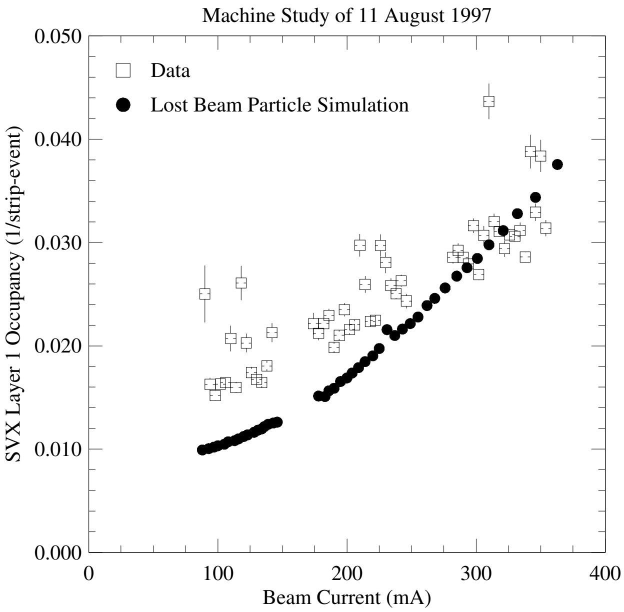

Figure 8: The occupancy in the first layer of the CLEO II.V SVX during HEP running. The prediction of the lost beam particle simulation and the measured data are shown.

factors. The occupancy measured in the SVX is a combination of beam-related occupancy and electronic noise effects. These electronic noise effects are measured with no beam in the machine, but are very sensitive to many other conditions. The electronic noise measured at zero beam current (0.009 hits/strip/event) has been added in quadrature with the beam-gas simulation hits to obtain the model prediction shown in the Figure. We also compare the occupancy prediction and measurement as functions of the detector tracking layer in Figure 9 for 300 mA total current. The electronic noise at zero beam current is determined for each layer and combined with the beam-gas simulation hits as described above. The agreement for the SVX (layers 1-3) is quite good – within a factor of two – while for the gas tracking devices (the remaining layers) is within measurement errors.

Note that in all these comparisons between the measured beam induced backgrounds and the simulation prediction, the contribution of synchrotron radiation is neglected. The effects of synchrotron radiation are not expected to penetrate beyond the second tracking layer and thus would only be observable in the radiation level and the first two layers of the SVX. In any case the simulation predicts that the contribution to SVX detector occupancy from synchrotron radiation during HEP running is negligible.

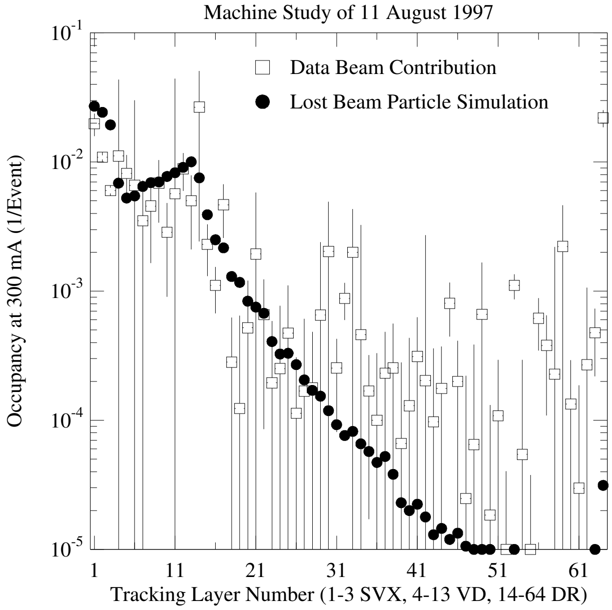

Figure 9: The occupancy as a function of tracking layer number in CLEO II.V during HEP running. The prediction of the lost beam particle simulation and the measured data are shown.

4.3 *Synchrotron Radiation*

Under normal HEP running the SR contribution to detector backgrounds cannot be detected. As mentioned above, simulation predicts the radiation dose from SR to be 8% that of lost particles, and the contribution to detector occupancy only 1%. Therefore, to observe SR or to compare with simulations it is necessary to adjust the orbit through the IR so that the beam is intentionally placed far off-axis in the IR quadrupoles in order to generate large SR fluxes.

As a machine studies experiment large SR fluxes were generated in two ways. In the first (case A), the crossing angle was increased from 2.0 mrad to 2.7 mrad (yielding a displacement of 19mm in Q1), and in the second (case B), a large amplitude bump was added to a reduced pretzel to yield $x'_{IP} = -1.9$ mrad and $x_{IP} = 2.7$ mm (yielding a displacement of 24 mm in Q1). For each measurement a single 10 mA bunch was used. The tunes were adjusted as needed to maintain good lifetime ($\tau > 1000$ min). In addition, the CsI radiation detectors were monitored to ensure that the particle backgrounds were maintained at a negligible level. The crossing angle and bump amplitude (needed for input to the SR background simulation) were obtained by fitting the orbits to separator kicks and magnetic corrector strengths respectively.

The trajectory for case A is shown in Figure 10. The incoming beam is bent in the strong horizontally focusing quadrupole Q1. The radiation fan from the central trajectory is shown by the upper and lower dotted lines. The beam is bent in Q0 (vertically focussing) and its radiation fan is shown by the lower and middle dotted lines. Thus,

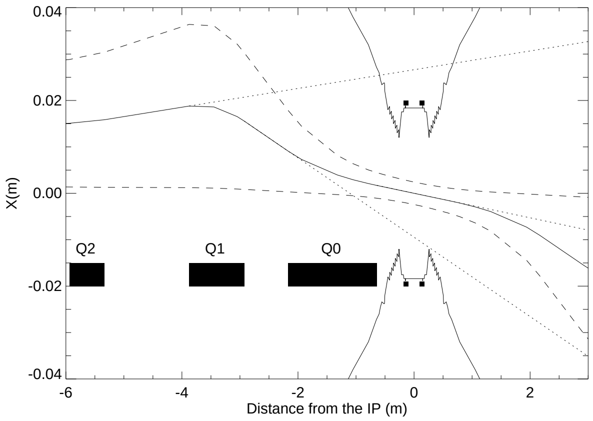

Figure 10: Trajectory for the synchrotron radiation machine studies experiment (case A). The interaction point is located at (0,0) on this plot. The beampipe radiation monitors are shown as black squares located at $(\pm 0.13, \pm 0.02)$. The "outside" of CESR is $+x$ and the "inside" is $-x$.

the mask tips on the outside of CESR are illuminated by Q1 radiation (from the core of the beam) and the downstream inside backscattering mask surface is illuminated by both Q1 and Q0 radiation (from beamsize).

The measured radiation distribution is compared to the Monte-Carlo simulation results in Figure 11. The highest radiation is observed in monitors 0-11 (downstream; $z > 0$ in Figure 10) and arises from SR which backscatters from the downstream mask surface. The monitors on the downstream end (0-11) have a larger solid angle from the mask surface than those on the upstream end (12-23) and those lying in the plane outside of CESR have the largest solid angle and therefore the largest radiation dose from x-ray fluorescence. The radiation on the upstream monitors is due primarily to tipscattering. The tips on the outside of CESR are illuminated by Q1 radiation. The upstream monitors therefore have the largest solid angle from the tip, and those on the inside have a larger solid angle than those on the outside.

The comparison for case B is shown in Figure 12. The trajectory is displaced even further in Q1, so event greater SR fluxes are generated. The radiation distribution is similar to that of the previous case. The agreement between the SR simulation and the data is quite good - typically within a factor of two. The experimental cases each test two different aspects of the SR simulation since the backscattering and tipscattering sources separately give rise to radiation in the downstream and upstream monitors respectively. Therefore, agreement for monitors 0-11 can be viewed as a test of the backscattering portion of the simulation while agreement for monitors 12-23 tests the tipscattering portion of the simulation.

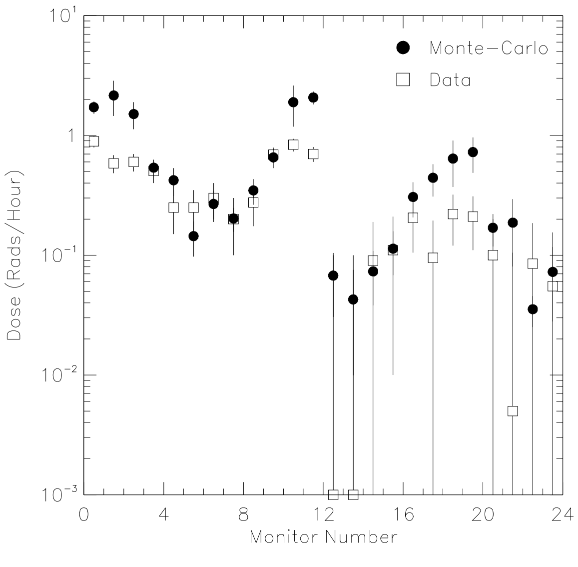

Figure 11: Beampipe radiation monitor response for the synchrotron radiation experiment labelled "case A." The monitors 0-11 are "downstream" in the experiment ($z > 0$ in Figure 10), and 12-23 are "upstream" ($z < 0$). The numbering is as follows: 0 and 12 are located in the plane of the machine on the *outside* of CESR, 3 and 15 are located on the top, 6 and 18 are located on the *inside* of CESR and 9 and 21 are located on the bottom.

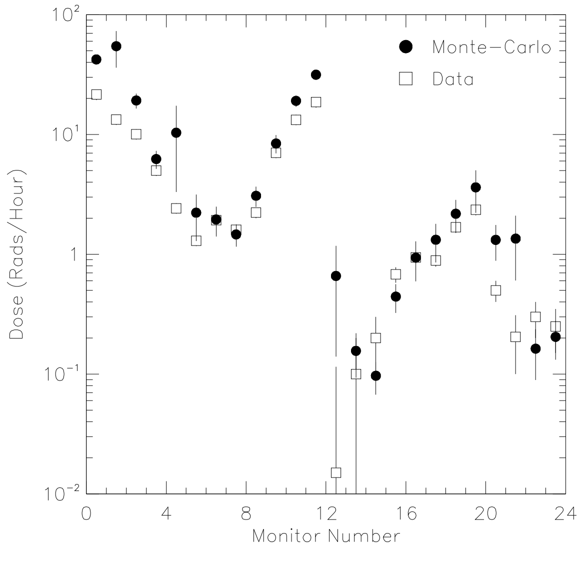

Figure 12: Beampipe radiation monitor response for the synchrotron radiation experiment labelled "case B."

5 CONCLUSION

The CESR/CLEO II.V interaction region has been described. The radiation dose measured by the IR radiation monitors during 172 weeks of operation is 22.2 krads, 12 krads of which was accumulated during HEP data-taking. Detailed comparisons of the background simulation with measured detector background and radiation dose have been performed. The agreement between measured and predicted radiation doses in the IR from beam-gas scattering is quite good, within $\sim$25% for the various experiments described. The comparison between beam-gas simulation and measured detector occupancies is in many ways more challenging. The agreement here is within a factor of two over a range in beam currents and better at higher currents. Synchrotron radiation is not readily observed during HEP running. The results of an experiment to generate a large SR dose were described and a comparison to simulation shows agreement within a factor of two in general, and much better in some cases. We are confident in the ability of these simulations to predict detector backgrounds at CESR and have based the design of the CESR Phase III IR shielding on them.

6 REFERENCES

[1] S. Henderson, Proc. 1997 Part. Acc. Conf., Vancouver BC, p.291.

[2] S. Henderson, Proceedings of the 2nd Workshop on Backgrounds at the Machine Detector Interface, ed. T. Browder and S. Sahu, Honolulu HI, 1997, World Scientific, p.6.

[3] Y. Kubota *et. al.* (CLEO Collaboration), NIM A320, (1992) 66.

[4] T. Hill, NIM A418, (1998) 32.

[5] S. Henderson, in these proceedings.

[6] J.P. Alexander *et. al.* NIM A337 (1993) 171.

[7] CESR-B Conceptual Design for a B-Factory Based on CESR, Cornell, June 1993.

[8] D. Cinabro, Proc. Workshop on Backgrounds at the Machine Detector Interface for B factories, UH 511-838-96, Hawaii, 1995.

[9] D. Cinabro, S. Henderson, H. Yamamoto, Int. Conf. High Energy Physics, Glasgow, 1994.

[10] D. Cinabro, Proc. 8th Meeting of DPF (Albuquerque, NM), World Scientific (1994).

[11] S. Henderson, Proc. 8th Meeting of DPF (Albuquerque, NM), World Scientific (1994).

[12] S. Henderson and S. Roberts, Proc. 1999 Part. Acc. Conf., New York, NY

[13] N. Mistry, Proc. Part Acc. Conf. 1997, Vancouver BC, p.3559.

[14] Y. Li, in these proceedings.

[15] Y. Li, private communication

[16] N. Mistry, Cornell CON 97-02.